Ultrastable Metallic Glasses *In Silico*

Anshul D. S. Parmar,[1] Misaki Ozawa,[2] and Ludovic Berthier[1,3]
[1]*Laboratoire Charles Coulomb (L2C), Université de Montpellier, CNRS, 34095 Montpellier, France*
[2]*Laboratoire de Physique Statistique, École Normale Supérieure, CNRS, PSL Research University, Sorbonne Université, 75005 Paris, France*
[3]*Department of Chemistry, University of Cambridge, Lensfield Road, Cambridge CB2 1EW, United Kingdom*

(Received 28 February 2020; accepted 24 July 2020; published 21 August 2020)

We develop a generic strategy and simple numerical models for multicomponent metallic glasses for which the swap Monte Carlo algorithm can produce highly stable equilibrium configurations equivalent to experimental systems cooled more than 10^7 times slower than in conventional simulations. This paves the way for a deeper understanding of the thermodynamic, dynamic, and mechanical properties of metallic glasses. As first applications, we considerably extend configurational entropy measurements down to the experimental glass temperature, and demonstrate a qualitative change of the mechanical response of metallic glasses of increasing stability toward brittleness.

DOI: 10.1103/PhysRevLett.125.085505

Glasses are obtained by cooling liquids into amorphous solids [1]. This process involves a rapidly growing relaxation time, making it difficult to investigate the nature of the glass transition in equilibrium [2,3]. Many types of materials can form glassy states, such as molecular, oxide, and colloidal glasses having various practical applications [4]. Among them, metallic glasses are a promising class known for higher strength and toughness [5], which is vital for applications. Computer simulations represent a valuable tool to investigate glass properties with atomistic resolution [3]. Model metallic glasses are widely used because they are simpler than molecular liquids to understand the basic mechanisms of the glass transition and accompany practical applications. However, typical cooling rates *in silico* are faster than in the laboratory by 6 to 8 orders of magnitude. Therefore, computer studies of metallic glasses may produce materials that behave differently from experimental systems. Our goal is to fill this wide gap for metallic glasses in order to access the thermodynamic, dynamic, and mechanical properties that can be directly compared to experiments.

Recently, the swap Monte Carlo algorithm has enabled the production of highly stable configurations for models of continuously polydisperse soft and hard spheres [6,7]. This was achieved by optimizing the size distribution and pair interactions to produce good glass-formers (preventing crystallization) with a massive thermalization speedup [7]. It was found, however, that previous popular models for metallic glasses, such as the Kob-Andersen [8] and Wahnström mixtures [9], are either not well suited for the swap algorithm [10] or crystallize too easily [7,11–14]. Further developments are clearly needed.

Here, we show how to develop multicomponent metallic glass-formers to benefit from the dramatic speedup offered by swap Monte Carlo and thus bridge the gap between metallic glass simulations and experiments [15–18]. Our strategy differs from earlier work [7] since it is inspired by the microalloying technique used in metallic glass experiments [19,20]. We introduce additional species to the original binary Kob-Andersen mixture to simultaneously improve its glass-forming ability [21,22] and swap efficiency [7]. This echoes the doping technique widely used in molecular liquids [23–25] to prevent crystallization [19,20,23,24]. The speedup provided by the swap Monte Carlo algorithm depends on the concentration of the doped species. For some models, we can produce for the first time equilibrium configurations of metallic glasses at the experimental glass transition temperature *in silico*. Our results pave the way for the next generation of thermodynamic and mechanical studies of metallic glasses using computer simulations.

Models.—The original Kob-Andersen (KA) model [8] is an 80:20 binary mixture of N_A Lennard-Jones particles of type A and N_B particles of type B, mimicking the mixture Ni-P. We add a new family of particles of type C, which can be a single type (ternary mixture) or several types (multicomponent). The pair interaction is

$$v_{\alpha_i\beta_j}(r) = 4\epsilon_{\alpha_i\beta_j}\left[\left(\frac{\sigma_{\alpha_i\beta_j}}{r}\right)^{12} - \left(\frac{\sigma_{\alpha_i\beta_j}}{r}\right)^{6}\right], \qquad (1)$$

where ϵ and σ are the energy scale and interaction range, respectively. We specify the particles index by Roman indices and the family type by Greek indices. The potential is truncated and shifted at the cutoff distance $r_{\mathrm{cut},ij} = 2.5\sigma_{\alpha_i\beta_j}$. For particles A and B, we use the interaction parameters of the original KA model: $\epsilon_{AB}/\epsilon_{AA} = 1.5$, $\epsilon_{BB}/\epsilon_{AA} = 0.5$, and $\sigma_{AB}/\sigma_{AA} = 0.8$,

$\sigma_{BB}/\sigma_{AA} = 0.88$. Energy and length are in units of ϵ_{AA} and σ_{AA}, respectively. Given the large size and energy disparities, performing particles swaps between A and B particles is prohibited [10], which leaves the standard KA model out of the recent swap developments.

We introduce N_C particles of type C. Each C particle is characterized by a continuous variable $\omega_i \in [0, 1]$ so that its interactions with A and B particles are given by

$$X_{AC} = \omega_i X_{AA} + (1 - \omega_i) X_{AB},$$
$$X_{BC} = \omega_i X_{AB} + (1 - \omega_i) X_{BB}, \quad (2)$$

where X stands for both ϵ and σ so that C particles are identical to A (B) particles when $\omega_i = 1$ (0) and smoothly interpolate between both species for $0 < \omega_i < 1$. Two C particles i and j interact between each other additively:

$$X_{C_i C_j} = \omega_{ij} X_{AA} + (1 - \omega_{ij}) X_{BB}, \quad (3)$$

where $\omega_{ij} = (\omega_i + \omega_j)/2$.

This generic framework offers multiple choices for the distribution of C particles, depending on the parameters N_C and on the chosen distribution $P(\omega)$ of the variable ω. We have explored two simple families, illustrated in Figs. 1(a) and 1(b). The first family, KA_1, is obtained using a flat distribution $P(\omega)$ on the interval [0, 1] [see Fig. 1(a)]. This corresponds to a multicomponent system where C particles continuously interpolate between A and B components. The second family, KA_2, is obtained by taking the opposite extreme where $P(\omega) = \delta(\omega - 1/2)$ [see Fig. 1(b)]. In that case, we simulate a discrete ternary mixture. In both cases, we define $\delta = N_C/(N_A + N_B)$ and consider a range of δ values from $\delta = 0\%$ (original KA mixture) up to $\delta = 20\%$. Contrary to previous work [7], the size dispersity quantified by the variance of the diameter distribution is nearly constant across the KA, KA_1, and KA_2 models. We perform simulations in a periodic cubic cell of volume V in three dimensions. All models are simulated at the number density $\rho = 1.2$, denoting the number of particles in unit volume σ_{AA}^3.

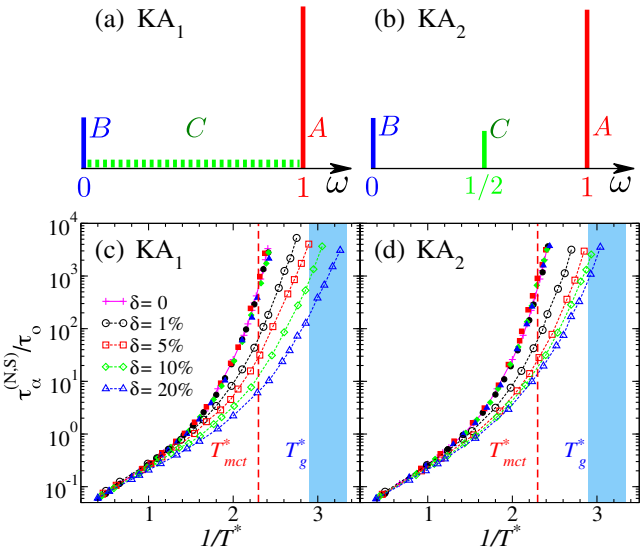

FIG. 1. (a),(b) Two families of Lennard-Jones models, composed of A and B particles interacting as in the KA model, and C particles intermediate between A and B types depending on the variable ω. The C particles improve the glass-forming ability and the efficiency of the swap Monte Carlo algorithm. Relaxation times for the (c) KA_1 and (d) KA_2 models using full $[\tau_\alpha^{(N)}]$ and empty $[\tau_\alpha^{(S)}]$ symbols. The blue box indicates the extrapolated location of the experimental glass transition temperature T_g^*, and $T_{\rm mct}^*$ is the mode-coupling crossover.

Swap Monte Carlo algorithm.—To achieve equilibration at very low temperatures, we perform Monte Carlo (MC) simulations possessing both translational displacements and particle swaps [26,27]. For the normal MC moves, a particle is randomly chosen and displaced by a vector randomly drawn within a cube of linear size $\delta r_{\rm max} = 0.15$. The move is accepted according to the Metropolis acceptance rule, enforcing detailed balance. Such MC simulations show quantitative agreement with molecular dynamics simulations in terms of glassy slow dynamics [28].

When using swap MC, we also perform particle swaps. We randomly choose a C particle, say particle i, characterized by ω_i. We then randomly choose a value $\Delta\omega$ in the interval $\Delta\omega = \pm 0.8$ and choose a second particle within this interval, say particle j. We estimate the energy cost to exchange the type of the two particles, $\omega_i \leftrightarrow \omega_j$, and accept the swap according to the Metropolis rule. In the swap MC scheme, we perform swap moves with probability $p = 0.2$ and translational moves with probability $1 - p = 0.8$. All parameters, $(\delta r_{\rm max}, p, \Delta\omega)$ have been carefully optimized to maximize the swap efficiency [see Supplemental Material [29] (SM)]. In particular, swaps with larger $\Delta\omega$ are essentially all rejected, confirming that direct A $\leftrightarrow$ B swaps are impossible. In essence, the C particles thus allow two-step exchanges such as A $\leftrightarrow$ C $\leftrightarrow$ B. Although we only apply this strategy to the KA model, we expect that it should generically apply to high-entropy alloys that have more than five components [39]. In both normal and swap MC schemes, one Monte Carlo time step represents N attempts to make an elementary move. Timescales are reported in this unit.

Glass-forming ability.—Thanks to modern computer resources, the original KA model is now found to be prone to crystallization [13,14,40]. We have repeated the detailed common neighbor analysis of Ref. [14]. We detected no sign of crystalline environments in our extended models, KA_1 and KA_2, across the wide temperature regime where thermalization can be achieved using the swap MC algorithm (see SM). Thus, the extended KA models developed here are much better glass-formers than the original KA model. Similarly to experiments, the doping C

particles considerably frustrate the system against crystallization [19,20,23,24].

Equilibration speedup.—The relaxation time τ_α of the system is quantified from the time decay of the self-intermediate scattering function for all particles, $F_s(q, t = \tau_\alpha) = 1/e$. We use $q = 7.34$, close to the first diffraction peak of the static structure factor. We respectively denote $\tau_\alpha^{(N)}$ and $\tau_\alpha^{(S)}$ the relaxation times for the normal (N) and swap (S) dynamics. We finally rescale the relaxation times using its value $\tau_o = \tau_\alpha^{(N)}(T = T_o)$ at the onset temperature T_o at which the relaxation time starts to deviate from the Arrhenius law.

We first concentrate on the physical dynamics using normal MC simulations for both models, KA_1 and KA_2, and various values of δ. We find that the temperature dependence of $\tau_\alpha^{(N)}$ for all models is very similar and is only weakly affected by the C particles (see SM). The presence of the C particles changes the energy or temperature scale from the original model. To account for this perturbation and ease the comparison between models, we introduce a rescaled temperature, $T^* = T(1 + \varepsilon(\delta))$, such that the data $\tau_\alpha^{(N)}$ vs $1/T^*$ for all models coincide [see Figs. 1(c) and 1(d); see also the $\tau_\alpha^{(N)}$ vs $1/T$ plots in SM]. The measured ε values reported in Table I are small and compatible with a linear growth, $\varepsilon(\delta) \simeq \delta$, suggesting that C particles simply act as a linear thermodynamic perturbation (see SM for KA_2). We confirm in SM that the pair structure is also weakly affected. From now on, we use the temperature scale T^* and thus, by definition, all models studied in this paper display the same physical (normal MC) dynamics as a function of T^*. They have the same reference temperatures as the original KA model: their onset temperature is $T_o^* \simeq 0.7$, and the mode-coupling crossover is at $T_{\rm mct}^* \simeq 0.435$. These conventional MC simulations can access $\tau_\alpha^{(N)}/\tau_o \sim 10^4$ for $N = 10^3$ particles, corresponding to the lowest simulated temperature $T_{\rm low}^* = 0.415$ and about ten days of CPU time. Following earlier work [7], we locate the experimental glass transition temperature T_g^* by extrapolating the measured dynamical data toward $\tau_\alpha^{(N)}/\tau_0 = 10^{12}$ using various functional forms that provide a finite range for its location. We find $T_g^* \in [0.3 - 0.345]$ (see Fig. 1) and suggest $T_g^* \approx 0.3$ as our favored estimate obtained using the parabolic law [41].

Our first important achievement follows from the temperature evolution of the relaxation times when using swap MC in Fig. 1. Whereas the original KA model with $\delta = 0$ can be thermalized down to $T_{\rm low}^* \approx 0.415$, we find that thermalization is achieved at much lower temperatures as soon as $\delta > 0$, with a speedup that *increases continuously and exponentially fast* with δ. For an equivalent numerical effort, we find for $\delta = 1\% - 20\%$, $T_{\rm low}^* = 0.306$–0.358 (for KA_1) and $T_{\rm low}^* = 0.326$–0.371 (for KA_2). The lowest temperature corresponds to $T_{\rm low}^* \approx 0.7 T_{\rm mct}^* \approx T_g^*$. Converting these temperatures into timescales, we estimate that the numerical speedup varies from a factor 10^2 for $\delta = 1\%$ up to more than 10^7 for $\delta = 20\%$. Thus, even a small amount of doping has a massive impact on the swap efficiency. The proposed metallic glass models considerably widen the accessible temperature regime available to computer simulations without suffering from crystallizations.

Configurational entropy.—We now characterize the configurational entropy, $s_c(T^*)$, of the very low temperature states produced with swap MC. We determine the configurational entropy from its conventional definition, $s_c(T^*) = s_{\rm tot}(T^*) - s_{\rm vib}(T^*)$ [42–45]. The equilibrium entropy, $s_{\rm tot}$, is straightforwardly measured by thermodynamic integration from the ideal gas to the studied state point [44]. The vibrational entropy, $s_{\rm vib}$, is obtained by a constrained Frenkel-Ladd [46] thermodynamic integration, generalized to properly quantify the mixing entropy contribution to the vibrational entropy [47]. This is a crucial point for the present models where polydispersity changes continuously with δ and alternate approaches—for instance, using inherent structures—would be inadequate [48]. Figure 2 shows the temperature evolution of the configurational entropy of KA_1 models. We use $T_{\rm mct}^*$ as a useful temperature scale to normalize both temperatures, $T^*/T_{\rm mct}^*$, and entropies, $s_c(T^*)/s_c(T_{\rm mct}^*)$, in the spirit of Kauzmann [42]. Our data for the KA model are consistent with previous work [49] and stop at $T_{\rm low}^*/T_{\rm mct}^* \approx 0.954$, where $s_c(T_{\rm low}^*)/s_c(T_{\rm mct}^*) \approx 0.93$, corresponding to the deepest states accessible with a conventional MC algorithm. Figure 2 shows that the thermalization speedup obtained by increasing δ is accompanied by a strong reduction of the configurational entropy. Hence, the deeply supercooled states obtained using swap MC correspond to

TABLE I. Characteristics of the KA_1 models. Scaling factor for the temperature ε, the lowest simulated temperature $T_{\rm low}^*$ relative to the mode-coupling crossover $T_{\rm mct}^*$, thermalization speedup, thermodynamic fragility K_T, and extrapolated Kauzmann temperatures T_K^*.

KA_1	$\delta = 0\%$	1%	5%	10%	20%
ε	0	0.01	0.08	0.13	0.25
$T_{\rm low}^*/T_{\rm mct}^*$	0.954	0.824	0.787	0.753	0.704
Speedup	1	10^2	6×10^3	8×10^4	2×10^7
K_T	0.335	0.334	0.312	0.293	0.274
T_K^*	0.252	0.246	0.236	0.224	0.210

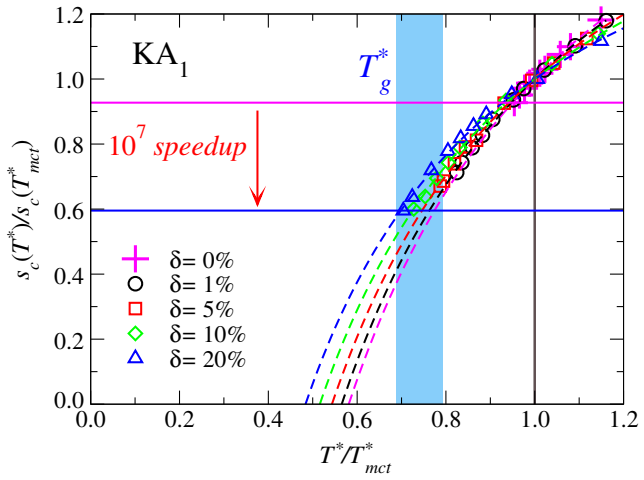

FIG. 2. Temperature evolution of configurational entropy using variables rescaled at the mode-coupling crossover temperature $T^*_{\rm mct}$. The horizontal lines correspond to the lowest accessible temperature for the original KA model and the $\delta = 20\%$ $\rm KA_1$ model.

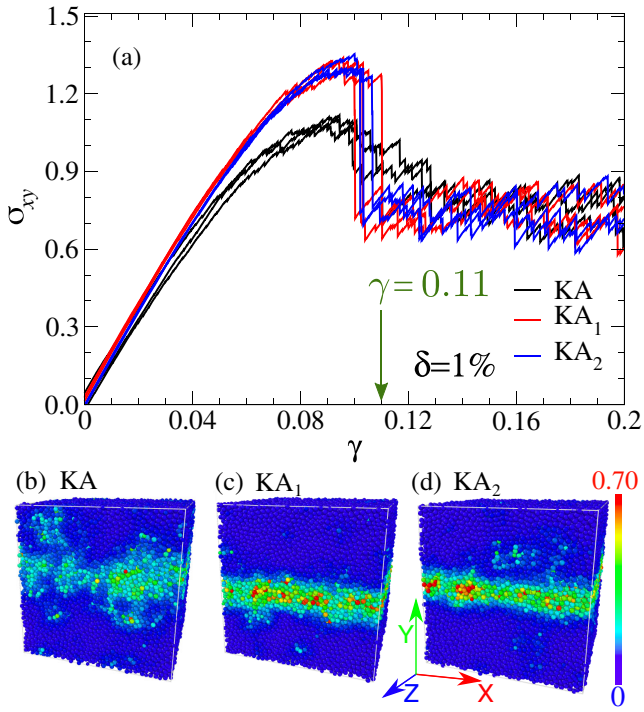

FIG. 3. (a) Stress-strain curves for three models—KA, $\rm KA_1$, and $\rm KA_2$—with $\delta = 1\%$. For each model, three individual realizations with $N = 50000$ are shown. (b)–(d) Snapshots of nonaffine displacement between $\gamma = 0$ and $\gamma = 0.11$ [vertical arrow in (a)] for KA (b), $\rm KA_1$ (c), and $\rm KA_2$ (d).

state points where much fewer amorphous packings are available to the system, which should translate into a larger point-to-set correlation length [50–52]. In earlier studies of the KA model, the putative Kauzmann transition was determined by fitting the decrease of s_c with the empirical form $s_c = A(1 - T^*_K/T^*)$, which also allows the determination of the thermodynamic fragility $K_T \equiv AT^*_K$ [53]. We extend this analysis to $\rm KA_1$ models and report T_K and K_T in Table I. Both quantities show a modest but systematic decrease with δ. Remarkably, after increasing the studied time window from 4 to 11 orders of magnitude (from $\delta = 0\%$ to 20%), the steep temperature dependence of s_c remains consistent with an entropy crisis taking place at $T_K \approx 0.5T^*_{\rm mct} > 0$. In particular, we detect no sign of a new mechanism to "avoid" it [54]. These data also contradict the arguments that models where swap MC works well are qualitatively distinct from those where it does not [55–57]. This finding constitutes our second important result.

Brittle yielding.—Turning to rheology, we demonstrate that accessing highly stable glassy configurations qualitatively affects how simulated metallic glasses yield. It was recently suggested that glass stability induces a ductile-to-brittle transition, confirmed numerically in a model for soft glasses [58–60]. Here, we establish that a similar transition exists in metallic glasses. To this end, we consider a larger system size, $N = 5 \times 10^4$, and apply the following preparation protocol for the original KA model and the $\delta = 1\%$ $\rm KA_1$ and $\rm KA_2$ models. First, we thermalize the system at high temperature, $T^* = 2.0$. Second, we instantaneously quench to the temperature $T^* = 0.373$ and 0.319 for KA and $\rm KA_{1,2}$, respectively, where $\tau^{(S)}_\alpha \simeq 10^{10}$ MC steps, and let them age during 10^6 swap MC steps. We expect to produce an ordinary computer glass of modest stability for the KA model but very stable configurations for $\rm KA_1$ and $\rm KA_2$ models. These aged glasses are quenched to $T = 0$ and sheared using a strain-controlled athermal quasistatic protocol [61]. We apply a uniform shear along the xy plane with strain increments $\Delta\gamma = 10^{-4}$. We measure the xy component of the shear stress, σ_{xy}, to obtain the stress-strain curves shown in Fig. 3(a). We visualize nonaffine particle displacements [62] in Figs. 3(b)–3(d).

For the KA model, the stress shows an initial quasilinear increase with small plastic events, a stress overshoot punctuated by many larger plastic events, and a gradual approach to steady state. Near yielding, plasticity is spatially heterogeneous but spreads over the entire system [see Fig. 3(b)] in agreement with previous findings [63–65]. For stable initial configurations, the stress overshoot transforms into a unique, sharp, macroscopic stress discontinuity [see Fig. 3(a)]. This brittle behavior is accompanied by a clear system-spanning shear band [see Figs. 3(c) and 3(d)]. The tendency to shear localization upon increasing stability is well-documented [66,67], but a genuine nonequilibrium discontinuous yielding transition only occurs for highly stable glassy systems [58] (see also Refs. [68–70]). These results extend to an experimentally relevant class of materials the observation that brittle yielding and macroscopic shear-band formation can be

studied in atomistic simulations. They also suggest the universality of the random critical point controlling the brittle-to-ductile transition [58]. This constitutes our third important result.

Perspectives.—The multicomponent models for metallic glasses developed here can be efficiently thermalized via swap Monte Carlo simulations down to temperatures that are not currently accessible to conventional simulation techniques and are comparable to the experimental glass transition. These models fill the gap between experimental and numerical works. Considering the extensive use made of the KA model [8], the improved glass-forming ability and thermalization efficiency will stimulate many future studies. Immediate applications concern further analysis of the thermodynamic, dynamical, and mechanical properties of the stable configurations obtained here to address questions regarding the Kauzmann temperature, the validity of the Adam-Gibbs relation (see SM for an initial attempt), and a microscopic description of shear-band formation and failure in metallic glasses. More broadly, the strategy proposed here is simple and versatile and can certainly be improved further. For example, increasing the number of components and their concentration allows the system to reach below T_g very efficiently (see SM for a four-component model). It could also be used to model some specific multicomponent materials (for instance, of the Ni-Pd-P type) and high-entropy alloys to deepen our theoretical understanding of metallic glasses and help the design of novel materials with specific properties.

We thank D. Coslovich and A. Ninarello for discussions and sharing data and codes. We also thank C. Cammarota, A. Liu, and S. Sastry for useful discussions. This work was supported by a grant from the Simons Foundation (No. 454933, L. B.).

[1] C. A. Angell, Science **267**, 1924 (1995).
[2] A. Cavagna, Phys. Rep. **476**, 51 (2009).
[3] L. Berthier and G. Biroli, Rev. Mod. Phys. **83**, 587 (2011).
[4] L. Berthier and M. Ediger, Phys. Today **69**, No. 1, 40 (2016).
[5] A. Greer, Y. Cheng, and E. Ma, Mater. Sci. Eng. Rep. **74**, 71 (2013).
[6] L. Berthier, D. Coslovich, A. Ninarello, and M. Ozawa, Phys. Rev. Lett. **116**, 238002 (2016).
[7] A. Ninarello, L. Berthier, and D. Coslovich, Phys. Rev. X **7**, 021039 (2017).
[8] W. Kob and H. C. Andersen, Phys. Rev. E **51**, 4626 (1995).
[9] G. Wahnström, Phys. Rev. A **44**, 3752 (1991).
[10] E. Flenner and G. Szamel, Phys. Rev. E **73**, 061505 (2006).
[11] Y. Brumer and D. R. Reichman, J. Phys. Chem. B **108**, 6832 (2004).
[12] R. Gutiérrez, S. Karmakar, Y. G. Pollack, and I. Procaccia, Europhys. Lett. **111**, 56009 (2015).
[13] T. S. Ingebrigtsen, J. C. Dyre, T. B. Schrøder, and C. P. Royall, Phys. Rev. X **9**, 031016 (2019).
[14] D. Coslovich, M. Ozawa, and W. Kob, Eur. Phys. J. E **41**, 62 (2018).
[15] H.-B. Yu, Y. Luo, and K. Samwer, Adv. Mater. **25**, 5904 (2013).
[16] D. P. Aji, A. Hirata, F. Zhu, L. Pan, K. M. Reddy, S. Song, Y. Liu, T. Fujita, S. Kohara, and M. Chen, arXiv:1306.1575.
[17] P. Luo, C. Cao, F. Zhu, Y. Lv, Y. Liu, P. Wen, H. Bai, G. Vaughan, M. Di Michiel, B. Ruta *et al.*, Nat. Commun. **9**, 1 (2018).
[18] T. Dziuba, Y. Luo, and K. Samwer, J. Phys. Condens. Matter **32**, 345101 (2020).
[19] W. H. Wang, Prog. Mater. Sci. **52**, 540 (2007).
[20] S. González, J. Mater. Res. **31**, 76 (2016).
[21] C. Tang and P. Harrowell, Nat. Mater. **12**, 507 (2013).
[22] K. Zhang, M. Wang, S. Papanikolaou, Y. Liu, J. Schroers, M. D. Shattuck, and C. S. O'Hern, J. Chem. Phys. **139**, 124503 (2013).
[23] C. Angell and D. Smith, J. Phys. Chem. **86**, 3845 (1982).
[24] K. Takeda, O. Yamamuro, I. Tsukushi, T. Matsuo, and H. Suga, J. Mol. Struct. **479**, 227 (1999).
[25] S. Tatsumi, S. Aso, and O. Yamamuro, Phys. Rev. Lett. **109**, 045701 (2012).
[26] D. Frenkel and B. Smit, *Understanding Molecular Simulation: From Algorithms to Applications*, Vol. 1 (Academic Press, Elsevier, San Diego, 2001).
[27] T. S. Grigera and G. Parisi, Phys. Rev. E **63**, 045102(R) (2001).
[28] L. Berthier and W. Kob, J. Phys. Condens. Matter **19**, 205130 (2007).
[29] See Supplemental Material, which includes Refs. [30–38], at http://link.aps.org/supplemental/10.1103/PhysRevLett.125.085505 for details about simulation methods, temperature scaling, determination of the experimental glass transition temperature, thermodynamics and its relation with dynamics, glass-forming ability, and an additional model system.
[30] S. Sastry, Phys. Rev. Lett. **85**, 590 (2000).
[31] S. Sastry, P. G. Debenedetti, and F. H. Stillinger, Phys. Rev. E **56**, 5533 (1997).
[32] J. D. Ferry, *Viscoelastic Properties of Polymers* (John Wiley & Sons, New York, 1980).
[33] M. Ozawa, C. Scalliet, A. Ninarello, and L. Berthier, J. Chem. Phys. **151**, 084504 (2019).
[34] M. P. Allen and D. J. Tildesley, *Computer Simulation of Liquids* (Oxford University Press, Oxford, 2017).
[35] G. Adam and J. H. Gibbs, J. Chem. Phys. **43**, 139 (1965).
[36] T. R. Kirkpatrick, D. Thirumalai, and P. G. Wolynes, Phys. Rev. A **40**, 1045 (1989).
[37] V. Lubchenko and P. G. Wolynes, Annu. Rev. Phys. Chem. **58**, 235 (2007).
[38] J. D. Honeycutt and H. C. Andersen, J. Phys. Chem. **91**, 4950 (1987).
[39] Y. Zhang, T. T. Zuo, Z. Tang, M. C. Gao, K. A. Dahmen, P. K. Liaw, and Z. P. Lu, Prog. Mater. Sci. **61**, 1 (2014).
[40] S. Toxvaerd, U. R. Pedersen, T. B. Schrøder, and J. C. Dyre, J. Chem. Phys. **130**, 224501 (2009).
[41] Y. S. Elmatad, D. Chandler, and J. P. Garrahan, J. Phys. Chem. B **114**, 17113 (2010).
[42] W. Kauzmann, Chem. Rev. **43**, 219 (1948).
[43] F. Sciortino, W. Kob, and P. Tartaglia, Phys. Rev. Lett. **83**, 3214 (1999).

[44] S. Sastry, J. Phys. Condens. Matter **12**, 6515 (2000).
[45] L. Berthier, M. Ozawa, and C. Scalliet, J. Chem. Phys. **150**, 160902 (2019).
[46] D. Frenkel and A. J. Ladd, J. Chem. Phys. **81**, 3188 (1984).
[47] M. Ozawa, G. Parisi, and L. Berthier, J. Chem. Phys. **149**, 154501 (2018).
[48] M. Ozawa and L. Berthier, J. Chem. Phys. **146**, 014502 (2017).
[49] A. Banerjee, M. K. Nandi, S. Sastry, and S. M. Bhattacharyya, J. Chem. Phys. **145**, 034502 (2016).
[50] J.-P. Bouchaud and G. Biroli, J. Chem. Phys. **121**, 7347 (2004).
[51] L. Berthier, P. Charbonneau, D. Coslovich, A. Ninarello, M. Ozawa, and S. Yaida, Proc. Natl. Acad. Sci. U.S.A. **114**, 11356 (2017).
[52] L. Berthier, P. Charbonneau, A. Ninarello, M. Ozawa, and S. Yaida, Nat. Commun. **10**, 1 (2019).
[53] S. Sastry, Nature (London) **409**, 164 (2001).
[54] C. P. Royall, F. Turci, S. Tatsumi, J. Russo, and J. Robinson, J. Phys. Condens. Matter **30**, 363001 (2018).
[55] M. Wyart and M. E. Cates, Phys. Rev. Lett. **119**, 195501 (2017).
[56] L. Berthier, G. Biroli, J.-P. Bouchaud, and G. Tarjus, J. Chem. Phys. **150**, 094501 (2019).
[57] V. Lubchenko and P. G. Wolynes, J. Phys. Chem. B **122**, 3280 (2017).
[58] M. Ozawa, L. Berthier, G. Biroli, A. Rosso, and G. Tarjus, Proc. Natl. Acad. Sci. U.S.A. **115**, 6656 (2018).
[59] M. Ozawa, L. Berthier, G. Biroli, and G. Tarjus, Phys. Rev. Research **2**, 023203 (2020).
[60] W.-T. Yeh, M. Ozawa, K. Miyazaki, T. Kawasaki, and L. Berthier, Phys. Rev. Lett. **124**, 225502 (2020).
[61] C. E. Maloney and A. Lemaître, Phys. Rev. E **74**, 016118 (2006).
[62] M. L. Falk and J. S. Langer, Phys. Rev. E **57**, 7192 (1998).
[63] M. Utz, P. G. Debenedetti, and F. H. Stillinger, Phys. Rev. Lett. **84**, 1471 (2000).
[64] M. Fan, M. Wang, K. Zhang, Y. Liu, J. Schroers, M. D. Shattuck, and C. S. O'Hern, Phys. Rev. E **95**, 022611 (2017).
[65] D. Rodney, A. Tanguy, and D. Vandembroucq, Model. Simul. Mater. Sci. Eng. **19**, 083001 (2011).
[66] F. Varnik, L. Bocquet, J.-L. Barrat, and L. Berthier, Phys. Rev. Lett. **90**, 095702 (2003).
[67] Y. Shi and M. L. Falk, Phys. Rev. Lett. **95**, 095502 (2005).
[68] J. Ketkaew, W. Chen, H. Wang, A. Datye, M. Fan, G. Pereira, U. D. Schwarz, Z. Liu, R. Yamada, W. Dmowski *et al.*, Nat. Commun. **9**, 1 (2018).
[69] G. Kapteijns, W. Ji, C. Brito, M. Wyart, and E. Lerner, Phys. Rev. E **99**, 012106 (2019).
[70] H. Bhaumik, G. Foffi, and S. Sastry,arXiv:1911.12957.